

# Kadanoff-Baym description of Hubbard clusters out of equilibrium: performance of many-body schemes, correlation-induced damping and multiple steady states.

M. Puig von Friesen, C. Verdozzi, and C.-O. Almbladh

*Mathematical Physics and European Theoretical Spectroscopy Facility (ETSF), Lund University, 22100 Lund, Sweden*

(Dated: November 21, 2021)

We present in detail a method we recently introduced (Phys. Rev. Lett. 103, 176404 (2009)) to describe finite systems in and out of equilibrium, where the evolution in time is performed via the Kadanoff-Baym equations within Many-Body Perturbation theory. The main non-equilibrium property we analyze is the time-dependent charge density. An other quantity we study is the exchange-correlation potential of time-dependent Density Functional Theory, obtained via reverse engineering from the time-dependent density. Our systems consist of small, strongly correlated clusters, described by a Hubbard Hamiltonian within the Hartree-Fock, second Born, GW and T-matrix approximations. We compare the results from the Kadanoff-Baym dynamics to those from exact numerical solutions. The outcome of our comparisons is that, among the many-body schemes considered, the T-matrix approximation is overall superior at all electron densities. Such comparisons permit a general assessment of the whole idea of applying Many-Body Perturbation Theory, in the Kadanoff-Baym sense, to finite systems. A striking outcome of our analysis is that when the system evolves under a strong external field, the Kadanoff-Baym equations develop a steady-state solution as a consequence of a correlation-induced damping. This damping is present both in isolated (finite) systems, where it is purely artificial, as well as in clusters contacted to (infinite) macroscopic leads. To illustrate this point we present selected results for a system coupled to contacts within the T-matrix and second Born approximation. This damping behavior is intrinsically linked to the Kadanoff-Baym time-evolution and is not a simple consequence of possible limitations/approximations in the calculation of the initial state. The extensive numerical characterization we performed indicates that this behavior is present whenever approximate self energies, based upon infinite partial summations, are used. A second important result is that, for isolated clusters, the steady state reached is not unique but depends on how one switches on the external field. Under some circumstances this is also true for clusters connected to macroscopic leads. We provide some statements of more general and conceptual character on how the damping mechanism depends on the system size and the number of particles, and conclude with an outlook and glimpses of future work.

PACS numbers: 71.10.-w 71.10.Fd 73.63.-b

## I. INTRODUCTION

The Kadanoff-Baym equations (KBE)<sup>1,2</sup> are one of the fundamental theoretical schemes of a microscopic description of quantum systems out of equilibrium.<sup>3,4</sup> Due the growing interest in time-dependent phenomena, in recent years the KBE have been the object of considerable attention in several branches of physics. Notable applications of the KBE are in the areas of molecular quantum transport, high energy coupled plasmas, nuclear matter, astrophysics, to mention a few.<sup>5-16</sup> Another favorable element to the widespread use of KBE is the constantly expanding capability of today's computers, which has made the full numerical solution of the KBE possible. A main strength of the KBE is that one can, in a constructive way, build approximations of increasing complexity for the one-particle Green's function,  $G$ , the key quantity in the KBE. These approximations are obtained via Many-Body Perturbation Theory (MBPT) and are known as conserving approximations, since they guarantee the conservation of important quantities such as total energy, number of particles, linear and angular momentum.

However, the fulfillment of such conserving conditions is no guarantee of the quality of the actual results ob-

tained within a specific MBA. Hence, it would be useful to have a way to assess the performance of a given conserving MBA. One of the aims of this paper is to evaluate the range of validity of a group of well known Many-Body Approximations (MBA:s) by comparing the one-particle densities with the exact results for finite strongly correlated clusters out of equilibrium. The main attractive feature of such comparisons to exact results is the possibility of scrutinizing the performance of the Many-Body Approximations in the non-equilibrium regime. This knowledge is most valuable if one wishes to use approximate many-body schemes for systems (typically, infinite ones, e.g. systems coupled to macroscopic leads as those we consider towards the end of the paper) where exact solutions are not available.

Describing small clusters with strong electronic correlations, and subject to time-dependent fields, presents interest not only from a conceptual point of view; there are very many instances where the technological relevance of cluster physics is manifestly evident.<sup>17,18</sup> The main focus of this work is to investigate the dynamics of finite clusters. In this regard, we provide here a detailed account of a study performed very recently,<sup>16</sup> producing additional results for clusters and presenting in great detail the methodology we developed. We will, however, present

some results for a system contacted to macroscopic contacts to generalize some of our main findings. Similar clusters to those discussed here, coupled to leads have already been considered either in the stationary limit<sup>11</sup> or in the real-time domain.<sup>13,14</sup>

As specific finite model systems, we consider open-ended linear chains<sup>19</sup> with short ranged Hubbard interactions. We study their dynamics through exact diagonalization methods and by propagating the KBE for different MBA:s. The approximations we consider are the Hartree-Fock (HFA), the second Born (BA), the GW (GWA)<sup>20</sup> and the T-matrix (TMA).<sup>21,22</sup> All these approximations are conserving,<sup>1</sup> which clearly is of great importance when propagating the KBE, and all of them, apart from HFA, have self energies which are non-local in space and time. For the GWA, we will consider both a spin-independent and a spin-dependent version.<sup>11,23</sup> The latter has the advantage to alleviate the effect of self-screening.<sup>24,25</sup>

A general outcome of our study is that the TMA is seen to perform better than the other MBS:s at all fillings and interaction strengths.

With the exact and KBE cluster dynamics at our disposal, we also investigate numerically a well established relation between MBPT and another framework to treat non-equilibrium phenomena, i.e. time-dependent Density Functional Theory (TDDFT).<sup>26,27</sup> Using a spin-independent TDDFT description for the spin-compensated Hubbard model,<sup>28</sup> we will obtain the exchange-correlation (xc) potentials corresponding to the different MBA:s via reverse engineering from the time-dependent densities.

Our results show that the time-dependent KBE present two interesting features. The first is that for large external fields, the KBE time evolution in clusters exhibits a damped behavior induced by many-body correlations (hereafter, we refer to this as correlation-induced damping). The second feature is that the steady state one reaches is not unique but depends on how the perturbation is switched on. We also investigate clusters connected to macroscopic leads, which we in this paper we treat within the TMA and BA. In this case the presence of the correlation-induced damping is in general not artificial but the steady states may be non-unique.

These statements are also valid in presence of macroscopic contacts, as shown below for a small cluster coupled to leads and with a time evolution within the TMA.

In finite clusters the correlation-induced damping and the existence of multiple steady states is artificial and we show that it is due to limitations of self-consistent Many-Body Perturbation theory when applied to finite systems. We will also provide selected numerical examples, which suggest that correlation-induced damping can be present even in the presence of leads.

The question whether or not the correlation-induced damping and the existence of multiple steady states in contacted systems is a mere consequence of MBPT is at present not so straightforward to address with full gen-

erality.

The paper is organized as follows: we start with a description of our model system(s) in section II; then, in section III, we discuss the general properties of the single-particle Green's function. Section IV is an overview of the Many-Body Approximations used in this work. Section V is devoted to the procedure to obtain the ground state within the KBE. How to solve the KBE for the time evolution is reported in section VI. In section VII we detail how we extract the TDDFT exchange-correlation potentials corresponding to a chosen MBA. The ground-state and time-dependent results are presented in section VIII and IX, respectively. Section X deals with the correlation-induced damping which occurs during the KBE time evolution and the existence of multiple steady states. Finally, in section XI we present our conclusions and direction for possible future work.

## II. MODEL SYSTEMS

We will consider one-dimensional clusters with  $M$  sites and with one orbital at each site. Thus, each site (or, equivalently, each orbital) can accommodate a maximum of two electrons, with opposite spin. The clusters may either be isolated, in which case the Hamiltonian in standard notation is (we set the on-site energies equal to 0)

$$H_C = -V \sum_{\langle RR' \rangle, \sigma} a_{R\sigma}^\dagger a_{R'\sigma} + U \sum_R \hat{n}_{R\uparrow} \hat{n}_{R\downarrow} + \sum_{R, \sigma} w_R(t) \hat{n}_{R\sigma}, \quad (1)$$

or they may be attached to non-interacting leads of infinite size, as discussed below. In Eq. (1),  $\hat{n}_{R\sigma} = a_{R\sigma}^\dagger a_{R\sigma}$ ,  $\sigma = \uparrow, \downarrow$ , and  $\langle RR' \rangle$  denotes pairs of nearest neighbor sites. The hopping parameter  $V = 1$  and  $w_R(t)$  is a local external field which can be of any shape in time  $t$  and space.  $U$  and  $w_R(t)$  are given in units of  $V$ . We will consider clusters with  $M = 2, 4, 6$  sites and, without leads,  $N_e = 2, 6$  electrons (in the presence of leads, the average number of electrons in the clusters is in general non-integer). Our approach is valid for systems which are compensated as well as uncompensated in spin. However, in what follows we will only consider clusters (with/out leads) with an equal average number of spin-up and -down electrons in the ground state; this will hold at all times during the dynamics, since  $H$  has no spin-flip terms. Henceforth,  $n = n_\uparrow = n_\downarrow$ , where,  $n_\sigma = N_\sigma/M$  and  $N_\sigma \equiv \langle \sum_{R \in C} \hat{n}_{R\sigma} \rangle$ . In the presence of leads,  $L$ , the Hamiltonian is

$$H = H_C + H_L + H_{LC} \quad (2)$$

where  $H_L$  describes non-interacting one-dimensional semi infinite chains,

$$H_L = -V_L \sum_{\substack{\langle RR' \rangle, \sigma \\ R, R' \in L}} a_{R\sigma}^\dagger a_{R'\sigma}, \quad (3)$$

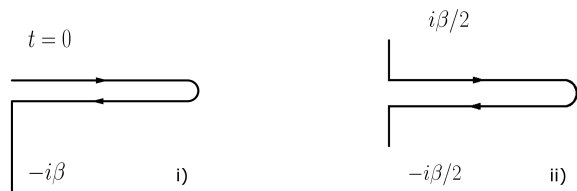


FIG. 1: Keldysh contours.

and  $H_{LC}$  describes hopping between the central region, C, and the leads

$$H_{LC} = -V_{LC} \sum_{\substack{\langle RR' \rangle, \sigma \\ R \in L, R' \in C}} a_{R\sigma}^\dagger a_{R'\sigma} + h.c. \quad (4)$$

For isolated clusters, we use a short iterative Lanczos propagation to obtain the exact time evolution. A description of our approach for approximate solutions in isolated and contacted clusters is the object of the next five sections.

### III. THE ONE-PARTICLE GREEN'S FUNCTIONS

The one-particle Green's function is a reduced quantity, containing much less information than the underlying wave function. In general, it describes a system connected to a bath with which energy and particle can be exchanged. The knowledge of the Green's function gives access to the expectation values of all single-particle operators, excitation energies and the total energy of the system.

The general definition of the one particle Green's function is

$$\mathcal{G}(\mathbf{r}_1\sigma_1z_1, \mathbf{r}_2\sigma_2z_2) = \langle \mathbf{r}_1\sigma_1 | \mathcal{G}(z_1, z_2) | \mathbf{r}_2\sigma_2 \rangle \quad (5)$$

$$-i \left\langle \hat{U}(-i\beta, 0) T_\gamma \left[ \hat{\psi}_H(\mathbf{r}_1\sigma_1z_1) \hat{\psi}_H^\dagger(\mathbf{r}_2\sigma_2z_2) \right] \right\rangle, \quad (6)$$

where  $\langle \dots \rangle$  denotes expectation values of the equilibrium ensemble,  $\hat{\psi}_H$  and  $\hat{\psi}_H^\dagger$  are the field operators in the Heisenberg picture,  $\gamma$  is the Keldysh contour, see Fig. 1(i,ii),  $T_\gamma$  is the path ordering operator,  $\hat{U}$  is an evolution operator and  $\beta = 1/k_B T$  is the inverse temperature of the bath. The  $\mathbf{r}$  and the  $s$  denote the labels corresponding to space (site) and spin coordinates of the single-particle basis. In this basis the Green's function becomes a matrix. The variable  $z$  belongs to the Keldysh contour and is in general complex. For notational convenience we denote real (imaginary) times by  $t$  ( $i\tau$ ). From the definition of the Green's function one can derive the so-called Kubo-Martin-Schwinger condition,<sup>29</sup>  $\mathcal{G}(z_1, z_2) = -\mathcal{G}(z_1, z_2 \pm i\beta)$ .

The expectation values of all the single-particle operators are obtained according to

$$\langle A(t) \rangle = -i \text{Tr} [A(t) \mathcal{G}(t, t^+)], \quad (7)$$

where the trace,  $\text{Tr} \equiv \sum_{\mathbf{r}_1\mathbf{r}_2\sigma\sigma'} \delta_{\mathbf{r}_1\mathbf{r}_2} \delta_{\sigma\sigma'}$ , is over space and spin indices. As discussed later and in the Appendix A, the total energy can be found by evaluating the Galitskii-Migdal or Luttinger-Ward functionals.

Since in this paper we study only paramagnetic systems in spin-independent fields, one-particle quantities such as the  $G$  and the  $\Sigma$  become spin-diagonal:

$$\mathcal{G}(\mathbf{r}_1\sigma_1z_1, \mathbf{r}_2\sigma_2z_2) = G(\mathbf{r}_1z_1, \mathbf{r}_2z_2) \delta_{\sigma_1\sigma_2}. \quad (8)$$

In the following, we will use the shorthand notation,  $1 = (\mathbf{r}_1, z_1)$ , etc., for space time coordinates.

The Green's function obeys an integral equation (the so-called Dyson equation)

$$G(12) = G_0(12) + \int_\gamma G_0(13) \Sigma(34) G(42) d34, \quad (9)$$

with the non-interacting Green's function  $G_0$  defined by

$$(i\partial_{z_1} - h(1)) G_0(12) = \delta(12). \quad (10)$$

In Eq. (10),  $h$  is the non-interacting Hamiltonian.<sup>30</sup> It is convenient to decompose  $h$  as  $h(t) = \hat{t} + w(t) - \mu$ , with i)  $\hat{t}$  the one-particle kinetic energy ( $-\nabla_1^2/2$  in coordinate space), ii)  $w(t)$  a local external field which may depend on time, and iii)  $\mu$  the chemical potential. The latter is taken to be in between the last occupied and the first non occupied levels. The inclusion of  $\mu$  in  $h$  implies that the Fermi energy is placed at zero energy; electron excitations thus have positive energies, while hole states have negative. The kernel of the Dyson equation,  $\Sigma$ , is called the self energy and is in general non-local in space and time. In the exact theory as well as in conserving approximations,<sup>1</sup> the self energy is a functional of the Green's function,  $\Sigma[G]$ , and the Dyson equation must thus be solved self-consistently. In equilibrium all quantities depend only on  $z = z_2 - z_1$  and the equations are then most easily handled, in terms of Fourier transformed quantities, in the frequency domain. There, the corresponding Dyson equation becomes a simple matrix equation, involving matrix multiplications; in the single-particle basis,

$$G(\epsilon) = G_0(\epsilon) + G_0(\epsilon) \Sigma(\epsilon) G(\epsilon). \quad (11)$$

In this paper, we will work only with systems for which the initial state is the actual ground state (i.e.  $\beta \rightarrow \infty$ ). That is, thermal mixtures ( $\beta < \infty$ ) of initial states will not be considered. In equilibrium, all two-point propagators can be expressed in terms of a spectral function. Specializing to the Green's function, the spectral decomposition has the form

$$G(\epsilon) = \int \frac{A(\epsilon')}{\epsilon' - \epsilon + i\eta \text{sgn}(\epsilon')} d\epsilon', \quad (12)$$

where the spectral function,  $A(\epsilon)$  is related to the anti-Hermitian part of the corresponding propagator, which

for the  $G$  is:  $A(\epsilon) = -\pi^{-1} [G(\epsilon) - G^\dagger(\epsilon)] \text{sgn}(\epsilon)$ . The Fermionic spectral function are positive definite and the one for  $G$  is normalized:

$$\int A(\epsilon) d\epsilon = 1, \quad (13)$$

where 1 represents the identity matrix in the single-particle basis.

#### IV. MANY-BODY APPROXIMATIONS

In general one can not construct the exact self energy and thus needs to rely on approximate schemes. In Many-Body Perturbation theory (MBPT), one can systematically construct self energies of increasing complexity. The main idea is making a diagrammatic expansion of the self energy, and selecting different classes of diagrams which are then summed up to infinite order. There is a very important group of approximations which conserve quantities such as the total energy, the number of particles, linear and angular momentum, when the system is subject to external fields. These conserving properties are related to the fact that the self energy is a functional derivative of a generating functional  $\Phi$ ,<sup>1</sup>

$$\Sigma(12) = \frac{\delta\Phi}{\delta G(21)}. \quad (14)$$

The use of conserving approximations is in general very important and, in fact, practically mandatory when studying non-equilibrium phenomena. In this paper we will study the conserving Hartree-Fock, second Born, GW and T-matrix approximations (HFA, BA, GWA and TMA respectively), see Fig. 2. The bare interaction is taken to be local in time,  $\mathcal{U}(\mathbf{r}_1, \mathbf{r}_2) \delta(t_1, t_2)$ . The formalism we will present is general but we remind the reader that in this paper we will only consider local interactions,  $\mathcal{U}(\mathbf{r}_1, \mathbf{r}_2) = U\delta(\mathbf{r}_1, \mathbf{r}_2)$  When specialized to our Hubbard clusters with one orbital/site (denoted by  $R$ ), the on-site interaction can be treated either as spin-dependent,  $U \sum_R n_{R\uparrow} n_{R\downarrow}$  or as spin-independent  $\frac{1}{2}U \sum_{R\sigma\sigma'} a_{R\sigma}^\dagger a_{R\sigma'}^\dagger a_{R\sigma'} a_{R\sigma}$ . These two ways are evidently equivalent in any order by order expansion such as the HFA or the BA. In approximations based upon partial summations, however, this equivalence may be lost. To illustrate this point we consider the GWA both spin-independently (GWA) and spin-dependently (SGWA). The TMA is treated only spin-dependently.

*Hartree-Fock approximation.* The simplest many-body treatment is given by the Hartree approximation (HA), where one takes only the first order direct term into account (i.e. the exchange is excluded). Due to its rather simple nature it will not be consider further.

The Hartree-Fock approximation (HFA) includes also the first order exchange diagram, the Fock term. The inclusion of this diagram, among other things, cures the self interaction of the HA. The resulting self energy is

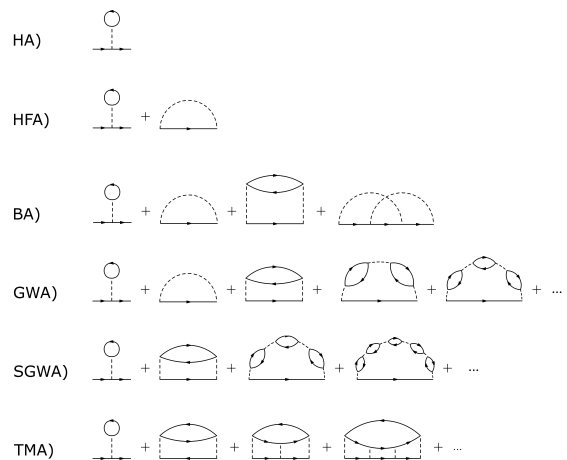


FIG. 2: Diagrammatic expansions of Many-Body Approximations.

local in time and thus constant in frequency space. The remaining diagrams are responsible for the many-body correlations and give rise to self energies which are non-local in time.

It is often convenient to separate the time-local HFA and correlation contributions and write

$$\Sigma(z_1, z_2) = \Sigma_{HF} \delta(z_1, z_2) + \Sigma_c(z_1, z_2). \quad (15)$$

*Second Born approximation.* The simplest scheme which involves correlations is the second Born approximation (BA) which corresponds to keeping all the diagrams up to second order.

*GW approximation.* The GW approximation is the leading term in the expansion of the self energy in terms of the dynamically screened interaction  $W$ . The expression for the self energy in time space is given by

$$\Sigma_{GW}(12) = \Sigma_H + iG(12)W(12). \quad (16)$$

It should be noted that this expression does not involve any matrix multiplication. The screening of the bare interaction,  $U$ , results from all possible electron-hole excitations which are described by a series of bubble diagrams, involving an irreducible polarization propagator,  $P$ . This series can be summed, yielding in frequency space, for a spin-independent interaction,

$$W = U + UPW \quad (17)$$

and, for a spin-dependent interaction,

$$\widehat{W} = UPU + (UP)^2 \widehat{W}. \quad (18)$$

We remind the reader that these Dyson like equations involve matrix multiplications. In both cases<sup>31</sup> the polarization propagator, in time space, is

$$P(12) = -iG(12)G(21). \quad (19)$$

*T-matrix approximation.* The T-matrix approximation comes from building the T-matrix,  $T$ , by summing all the ladder diagrams, representing electron-electron or hole-hole scattering.<sup>32</sup> The expression for the self energy is given by

$$\Sigma_{TM}(12) = \Sigma_{HF} + i \int \mathcal{U}(13) G(43) T(34) \mathcal{U}(42) d34. \quad (20)$$

In the case of an on-site, site-independent interaction this simplifies to

$$\Sigma_{TM}(12) = \Sigma_{HF} + iU^2 G(21) T(12). \quad (21)$$

The sum of the ladder terms in the T-matrix results in

$$T = \phi - \phi \mathcal{U} T, \quad (22)$$

where the so-called irreducible vertex  $\phi$  is defined as

$$\phi(12) = -iG(12)G(21). \quad (23)$$

## V. GROUND STATE

The ground state is obtained by solving the Dyson equation, Eq. (11) self-consistently. For clusters contacted to non-interacting leads, the problem can be expressed entirely in terms of propagators which refer only to the central region and an embedding self energy,<sup>33,34</sup>

$$\Sigma_{emb}(\epsilon) = \sum_L |V_{LC}|^2 \tilde{g}_L(\epsilon), \quad (24)$$

where  $\tilde{g}_L(\epsilon)$  is the non-interacting Green's function of the uncontacted lead  $L$ . The full Green's function in the central region will now obey a Dyson equation with both a many-body and an embedding self energy. The presence of  $\Sigma_{emb}$  gives rise to continuous spectra, and standard techniques can be used to find self-consistent solutions.

For the isolated clusters, we used a meromorphic representation to be described below.

### A. Meromorphic representation of finite systems

For convenience all one-body quantities are represented as matrices in a single-particle basis, e.g.  $G_{RR'}(\epsilon) = \langle R | G(\epsilon) | R' \rangle$ . In a finite system with a finite phase space, all the spectral functions are discrete:

$$A_{RR'}(\epsilon) = \sum_j A_{RR'}^j \delta(\epsilon - a_j), \quad (25)$$

where  $A_{RR'}^j$  is a residue matrix and  $a_j$  is a pole position.

From Eq. (12) we see that the propagators themselves become meromorphic,

$$G_{RR'}(\epsilon) = \sum_j \frac{A_{RR'}^j}{\epsilon - a_j + i\eta \text{sgn}(\epsilon)}. \quad (26)$$

One main advantage in using a meromorphic representation is that convolutions and cross-correlations are made analytically.<sup>35</sup> Given the two functions

$$A_{RR'}(\epsilon) = \sum_j \frac{A_{RR'}^j}{\epsilon - a_j}, \quad B_{RR'}(\epsilon) = \sum_j \frac{B_{RR'}^j}{\epsilon - b_j}, \quad (27)$$

then their cross-correlation

$$C_{RR'}(\epsilon) = \int A_{RR'}(\epsilon') B_{RR'}(\epsilon + \epsilon') \frac{d\epsilon'}{2\pi i}, \quad (28)$$

becomes

$$C_{RR'}(\epsilon) = \sum_{j k} A_{RR'}^k B_{RR'}^j \frac{1}{\epsilon + a_k - b_j}. \quad (29)$$

A second important attractive feature of a meromorphic representation is that one can compute at once the equilibrium many-body quantities with any time argument, both real and imaginary. For our Hubbard clusters, each of the quantities  $G, \Sigma, P, W, \Phi, T$  will be expressed in such representation during in the actual calculations.

### B. Solution to the Dyson equation

The solution to the Dyson equation for the  $G$  can formally be written<sup>36</sup>

$$G(\epsilon) = [G_0^{-1}(\epsilon) - \Sigma(\epsilon)]^{-1} = [\epsilon - h - \Sigma(\epsilon)]^{-1}. \quad (30)$$

The solution of this matrix equation is obtained in two steps<sup>35</sup>: 1) search of the pole position and 2) calculation of the residue matrix.

1) The pole positions of  $G$  correspond to the zeros of

$$\det[\epsilon - h - \Sigma(\epsilon)], \quad (31)$$

which we find by ordinary root finding algorithms.

2) Once the pole positions are found we calculate the residue matrices by integration in the complex plain. We have in general

$$\oint f(\epsilon) = 2\pi i \sum_j \text{Res}(f, a_j), \quad (32)$$

where

$$f(\epsilon) = \sum \frac{A_j}{\epsilon - a_j}. \quad (33)$$

If we now perform a closed integration around the pole  $a_j$  we obtain directly the residue matrix

$$A_j = \frac{1}{2\pi i} \oint_{a_j} f(\epsilon). \quad (34)$$

This integration is, in practice, performed numerically.

### C. Self-consistency

To reach self-consistency, we start by constructing the self energy with some initial  $G$ , normally taken to be  $G_0$ , and then solve the corresponding Dyson equation. The resulting  $G$  is then used to build the new self energy and the procedure is carried on until convergence. In order to keep the number of poles under control (such number increases rapidly from iteration to iteration), we make use of a "decimation" procedure, where poles are merged if there are small or close enough. When two poles are merged, the new pole position is the old center of mass position ("mass" being the trace of the residue matrix) and the new residue matrix is the sum of the two old residue matrices. To improve the convergence we update  $G$  by making a linear combination of the new (solution of the Dyson equation) and the old  $G$ 's. There are different functionals which yield the total energy of a system, all of which are equivalent at the point of stationary solution to the Dyson equation. However, away from self-consistency, they do in general not coincide. One independent way of evaluating the degree of self-consistency is thus by comparing the values of different energy functionals, see appendix A.

## VI. TIME DEPENDENCE

When an external field is applied to a system, it is in general driven out of equilibrium. When the system is out of equilibrium and away from the steady-state regime, all the quantities will intrinsically depend on the two time arguments ( $t_1, t_2$ ) separately and the Keldysh formalism becomes essential. To explicitly show which convention we used in this paper for the path-ordered two-point Keldysh functions,  $\mathcal{K}$ , we give some definitions. A general Keldysh function can be written

$$\mathcal{K}(12) = \mathcal{K}^\delta(12) \delta(z_1, z_2) + \Theta(12) \mathcal{K}^>(12) + \Theta(21) \mathcal{K}^<(12), \quad (35)$$

where  $>$  ( $<$ ) refers to the hole (electron) part, and  $\mathcal{K}^\delta$  the time-local part.

The time coordinates are on the Keldysh contour and may be real or complex. For real times we may also introduce retarded and advanced propagators,

$$\mathcal{K}^R(12) = \mathcal{K}^\delta(12) \delta(z_1, z_2) + \Theta(t_1, t_2) [\mathcal{K}^>(12) - \mathcal{K}^<(12)], \quad (36)$$

$$\mathcal{K}^A(12) = \mathcal{K}^\delta(12) \delta(z_1, z_2) - \Theta(t_2, t_1) [\mathcal{K}^>(12) - \mathcal{K}^<(12)]. \quad (37)$$

Note that for the  $\mathcal{K}$ 's considered in the paper, only  $\Sigma$  and  $W$  have parts which are local in time.

When both time arguments are imaginary, the Keldysh function reduces to the corresponding equilibrium Matsubara function:

$$\mathcal{K}^M(\tau - \tau') = -i\mathcal{K}(-i\tau, -i\tau'). \quad (38)$$

In Eq. (35),  $\Theta$  (12) should be understood as  $\Theta(z_1, z_2)$ , a generalized Heaviside function for  $z_1, z_2$  on the ordered Keldysh contour. It is worth noting that when both time arguments lie on the imaginary (Matsubara) axis, the quantities represent the initial, equilibrium, state which depend only on the time differences. As an example of how these terms are found in equilibrium in the meromorphic representation we display the hole contribution to the Green's function:

$$G^<(t_1, t_2) = i \sum_{j < \mu} A_j e^{ia_j(t_1 - t_2)} \quad (39)$$

when both time arguments are real,

$$G^<(t, -i\tau) = i \sum_{j < \mu} A_j e^{ia_j t} e^{a_j \tau} \quad (40)$$

when both one time argument is real and one imaginary,

$$G^<(-i\tau_1, -i\tau_2) = i \sum_{j < \mu} A_j e^{-a_j(\tau_1 - \tau_2)} \quad (41)$$

when both time arguments are imaginary.

### A. General symmetries

We recall some prominent symmetry relations which will be used during the time propagation. From the definition of the Green's function, Eq. (6), one can derive a very important symmetry,<sup>37</sup> which enters many relevant and useful relations:

$$G^{\gtrless}(12) = -G^{\gtrless}(21)^\dagger. \quad (42)$$

Additionally, from the definition of the retarded and advanced Green's functions we obtain

$$G^{R/A}(12) = G^{A/R}(21)^\dagger. \quad (43)$$

From the expansion of the  $T$  and  $W$  in terms of  $\phi$  and  $P$  it follows that the  $T$  and  $W$  will have the same symmetry properties as  $\phi$  and  $P$ . The symmetries of  $\phi$  and  $P$  can be deduced from their definitions

$$P^{\gtrless}(12) = -P^{\gtrless}(21)^\dagger \implies W^{\gtrless}(12) = -W^{\gtrless}(21)^\dagger \quad (44)$$

and

$$\phi^{\gtrless}(12) = -\phi^{\gtrless}(21)^\dagger \implies T^{\gtrless}(12) = -T^{\gtrless}(21)^\dagger. \quad (45)$$

In a similar way we find a symmetry relation, valid for all approximations, for the self energy,

$$\Sigma^{\geq}(12) = -\Sigma^{\geq}(21)^{\dagger}. \quad (46)$$

An additional symmetry fulfilled by  $W$  is

$$W^{\geq}(12) = W^{\leq}(21), \quad (47)$$

which implies

$$W^>(z, z) = W^<(z, z), \quad \text{Re } W_{RR'}(z, z) = 0 \quad \forall R, R'. \quad (48)$$

No equivalent relation exists for  $T$ .

### B. Solving for the non-equilibrium Green's function

To obtain the non-equilibrium Green's function we need to solve the corresponding equations of motion, called the Kadanoff-Baym equations (KBE),

$$(i\partial_{t_1} - h(1))G(12) = \delta(12) + \int_{\gamma} \Sigma(13)G(32) d3, \quad (49)$$

$$(-i\partial_{t_2} - h(2))G(12) = \delta(12) + \int_{\gamma} G(13)\Sigma(32) d3. \quad (50)$$

The kernel of these equations, the  $\Sigma$ , will in general be a contraction of the Green's function with another quantity which involves an infinite order summation such as the  $T$  or  $W$ . These quantities are defined by corresponding integral equations. Specializing to the case of  $T$ , we have

$$T(12) = \Phi(12) - \int_{\gamma} \Phi(13)\mathcal{U}(34)T(42) d34, \quad (51)$$

$$T(12) = \Phi(12) - \int_{\gamma} T(13)\mathcal{U}(34)\Phi(42) d34. \quad (52)$$

We thus have two sets of coupled integral equations which need to be solved simultaneously at all times.

### C. Solution of coupled integral equations

From the symmetry relations Eqs. (42, 44, 45) we see that  $G$  and  $W, T$  are only needed on the upper/lower time matrix. We choose the lesser components on the upper triangle  $t_1 \geq t_2$  and the greater ones on the lower triangle  $t_1 < t_2$ .<sup>38</sup> Propagation is thus made by expanding the Keldysh functions on the time square from  $T$  to  $T + \Delta$ , see Fig. 3. In the integral equations, Eqs. (49, 50, 51, 52), the function to be determined appears in both the right and left-hand sides. To solve these equations we use a self-consistent predictor-corrector method.<sup>39</sup> The method can be described schematically by an external loop, where an approximate  $\bar{G}$  at  $T + \Delta$  is generated by propagating Eqs. (49, 50), and an internal loop, where

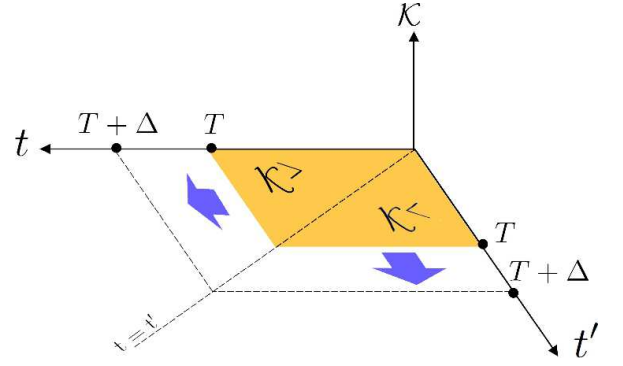


FIG. 3: (Color online) Time square.

Eqs. (51, 52) are solved self consistently for a fixed kernel  $\phi[\bar{G}]$ . The external loop is performed by a predictor-corrector method described below while the internal one is solved by the same iteration method as described for the ground state. The external loop is initiated by an extrapolated value of the collision integrals  $\int_{\gamma} \Sigma_c G$ , whilst the internal loop is started by an extrapolated value of the  $W, T$ . The new time step is generated when the external loop achieves self-consistency.

### D. Kadanoff-Baym equations

When propagating the Green's functions it is convenient to separate the terms which are local in time and single-particle like ( $h$  and  $\Sigma_{HF}$ ) from the remaining correlation-induced ones<sup>39</sup> and introduce

$$\mathfrak{h} = h + \Sigma_{HF}. \quad (53)$$

In this way,  $\mathfrak{h}$  substitutes  $h$  and the full self energy is replaced by its correlation part  $\Sigma_c$  in the KBE (*cf.* Eqs. (49, 50)). The reason for this partitioning is twofold: on the one hand the contribution from the single particle evolution is very important (and could thus lead to large numerical errors in the correlation contribution) and on the other it can be solved essentially in an exact way as will be detailed in Sec VIF.

There are several equivalent contours on which one can define the KBE. We use the contour ii) in Fig. 1, which is numerically more stable and has an analytical limit when the temperature goes to zero. Once we specialize to this contour, the KBE become

$$i\partial_{t_1} G^{\leq}(t_1, t_2) = \mathfrak{h}(t_1) G^{\leq}(t_1, t_2) + I_1^{\leq}(t_1, t_2), \quad (54)$$

$$-i\partial_{t_2} G^{\leq}(t_1, t_2) = G^{\leq}(t_1, t_2) \mathfrak{h}(t_2) + I_2^{\leq}(t_1, t_2), \quad (55)$$

$$i\partial_t G^<(t, -i\tau) = \mathfrak{h}(t) G^<(t, -i\tau) + I^<(t, -i\tau), \quad (56)$$

$$-i\partial_t G^>(-i\tau, t) = G^>(-i\tau, t) \mathfrak{h}(t) + I^>(-i\tau, t), \quad (57)$$

where the collision integrals with both time arguments

real are

$$I_1^{\lessgtr}(t_1, t_2) = \int_0^{t_1} d\bar{t} \left[ \Sigma_c^R(t_1, \bar{t}) G^{\lessgtr}(\bar{t}, t_2) + \Sigma_c^{\lessgtr}(t_1, \bar{t}) G^A(\bar{t}, t_2) \right] \\ + \frac{1}{i} \int_0^{\beta/2} d\bar{\tau} \left[ \Sigma_c^{\lessgtr}(t_1, -i\bar{\tau}) G^{\lessgtr}(-i\bar{\tau}, t_2) + \Sigma_c^{\lessgtr}(t_1, i\bar{\tau}) G^{\lessgtr}(i\bar{\tau}, t_2) \right], \quad (58)$$

$$I_2^{\lessgtr}(t_1, t_2) = \int_0^{t_2} d\bar{t} \left[ G^R(t_1, \bar{t}) \Sigma_c^{\lessgtr}(\bar{t}, t_2) + G^{\lessgtr}(t_1, \bar{t}) \Sigma_c^A(\bar{t}, t_2) \right] \\ + \frac{1}{i} \int_0^{\beta/2} d\bar{\tau} \left[ G^{\lessgtr}(t_1, -i\bar{\tau}) \Sigma_c^{\lessgtr}(-i\bar{\tau}, t_2) + G^{\lessgtr}(t_1, i\bar{\tau}) \Sigma_c^{\lessgtr}(i\bar{\tau}, t_2) \right]. \quad (59)$$

The collision integrals with one of the time arguments complex specialize to

$$I^<(t, -i\tau) = \int_0^t d\bar{t} \Sigma_c^R(t, \bar{t}) G^<(\bar{t}, -i\tau) \\ + \int_0^{\beta/2} d\bar{\tau} \left[ \Sigma_c^<(t, -i\bar{\tau}) G^M(\bar{\tau} - \tau) + \Sigma_c^>(t, i\bar{\tau}) G^M(-(\bar{\tau} + \tau)) \right], \quad (60)$$

$$I^>(-i\tau, t) = \int_0^t d\bar{t} G^>(-i\tau, \bar{t}) \Sigma_c^A(\bar{t}, t) \\ + \int_0^{\beta/2} d\bar{\tau} \left[ G^M(\tau - \bar{\tau}) \Sigma_c^>(-i\bar{\tau}, t) + G^M(\tau + \bar{\tau}) \Sigma_c^<(i\bar{\tau}, t) \right]. \quad (61)$$

It is worth noting that all Eqs. (58 - 60) contain terms which involve integration along the Matsubara (vertical) axis and which represent the memory of initial state correlations during the time evolution.

For the collision integrals, one can derive a similar symmetry property:

$$I_1^{\lessgtr}(12) = -I_2^{\lessgtr}(21)^\dagger. \quad (62)$$

An important consequence of this relation is that the densities<sup>40</sup> are manifestly real. From the KBE one can derive that the condition for real densities is given by

$$[I_1^<(t, t) - I_2^<(t, t)] = [I_1^<(t, t) - I_2^<(t, t)]^\dagger, \quad (63)$$

which is manifestly satisfied by Eq. (62). Furthermore, on the time diagonal, we obtain another relation, which is very useful in from the computationally point of view:

$$I_{1/2}^{\lessgtr} = I_{1/2}^{\gtrless}. \quad (64)$$

From the properties of integral equations, it follows that all the symmetry and structure properties of the Green's function are those of  $G_0$ .

The discussion of the KBE above is valid for extended and finite systems alike. When the interaction is confined to a central region which is contacted to possibly

macroscopic leads, the problem can again be expressed in propagators which refer only to the central region, and an embedding self energy which now depends on time,<sup>13,14</sup>

$$\Sigma_{emb}(t_1, t_2) = \sum_L |V_{LC}|^2 \tilde{g}_L(t_1, t_2). \quad (65)$$

Here  $\tilde{g}_L(t_1, t_2)$  is the non-interacting Green's function of the uncontacted lead  $L$ , possibly subject to a uniform but time-dependent bias. The full Green's function in the central region will now obey the KBE with both the self energy from the interaction and the one from the leads via the embedding. The embedding self energy is entirely non-local in time and will be treated on the same footing as the correlation part of the interaction self energy. It is worth noting that the embedding self energy involve no self-consistency and can thus be calculated once the external bias (if present) is known.

### E. The Dyson equation for $T$ and $W$

Propagating in time the KBE within a specific MBA-based partial summation, requires solving a Dyson equation for auxiliary quantities which enter the expression for the self energy. For the TMA and GWA such quantities are the  $T$  and  $W$ , respectively. The components of the corresponding Dyson equations (again specialized to the case of  $T$ ) Eqs. (51, 52) are, for both times on the real axis,

$$T^{\lessgtr}(t_1, t_2) = \Phi^{\lessgtr}(t_1, t_2) \\ - \int_0^{t_1} d\bar{t} \left[ \Phi^R(t_1, \bar{t}) \mathcal{U} T^{\lessgtr}(\bar{t}, t_2) + \Phi^{\lessgtr}(t_1, \bar{t}) \mathcal{U} T^A(\bar{t}, t_2) \right] \\ - \frac{1}{i} \int_0^{\beta/2} d\bar{\tau} \left[ \Phi^<(t_1, -i\bar{\tau}) \mathcal{U} T^>(-i\bar{\tau}, t_2) + \Phi^>(t_1, i\bar{\tau}) \mathcal{U} T^<(i\bar{\tau}, t_2) \right], \quad (66)$$

$$T^{\gtrless}(t_1, t_2) = \Phi^{\gtrless}(t_1, t_2) \\ - \int_0^{t_2} d\bar{t} \left[ T^R(t_1, \bar{t}) \mathcal{U} \Phi^{\gtrless}(\bar{t}, t_2) + T^{\gtrless}(t_1, \bar{t}) \mathcal{U} \Phi^A(\bar{t}, t_2) \right] \\ - \frac{1}{i} \int_0^{\beta/2} d\bar{\tau} \left[ T^<(t_1, -i\bar{\tau}) \mathcal{U} \Phi^>(-i\bar{\tau}, t_2) + T^>(t_1, i\bar{\tau}) \mathcal{U} \Phi^<(i\bar{\tau}, t_2) \right], \quad (67)$$

when one of the time arguments is imaginary we have

$$T^<(t, -i\tau) = \Phi^<(t, -i\tau) - \int_0^t d\bar{t} \Phi^R(t, \bar{t}) \mathcal{U} T^<(\bar{t}, -i\tau) \\ - \int_0^{\beta/2} d\bar{\tau} \left[ \Phi^<(t, -i\bar{\tau}) \mathcal{U} T^M(\bar{\tau} - \tau) + \Phi^>(t, i\bar{\tau}) \mathcal{U} T^M(-(\bar{\tau} + \tau)) \right], \quad (68)$$

$$\begin{aligned}
T^>(-i\tau, t) &= \Phi^>(-i\tau, t) - \int_0^t d\bar{t} T^>(-i\tau, \bar{t}) \mathcal{U} \Phi^A(\bar{t}, t) \\
&- \int_0^{\beta/2} d\bar{\tau} \left[ T^M(\tau - \bar{\tau}) \mathcal{U} \Phi^>(-i\bar{\tau}, t) + T^M(\tau + \bar{\tau}) \mathcal{U} \Phi^<(i\bar{\tau}, t) \right].
\end{aligned} \tag{69}$$

### F. Time propagation algorithm

As mentioned in section VID we treat the time-local part of the self energy ( $\Sigma_{HF}$ ) on the same footing as the non-interacting terms ( $h$ ) in the time propagation. The evolution from these single-particle terms can be expressed in terms of a single-particle evolution operator  $S$  which is a time-dependent matrix in single-particle labels. This leads to the following unitary gauge transformation

$$G^{\lessgtr}(t_1, t_2) = S(t_1, 0) g^{\lessgtr}(t_1, t_2) S^\dagger(t_2, 0), \tag{70}$$

where  $S$  satisfies the following differential equation:

$$i\partial_{t_1} S(t_1, 0) = \mathfrak{h}(t_1) S(t_1, 0), \tag{71}$$

with the initial condition

$$S(0, 0) = S^\dagger(0, 0) = 1 \tag{72}$$

and the group property

$$S(t_1, \bar{t}) S(\bar{t}, t_2) = S(t_1, t_2). \tag{73}$$

Specializing to the case of  $G^>$ , we get:

$$\begin{aligned}
i\partial_{t_1} G^>(t_1, t_2) &= \mathfrak{h}(t_1) S(t_1, 0) g^>(t_1, t_2) S^\dagger(t_2, 0) \\
&+ S(t_1, 0) i\partial_{t_1} g^>(t_1, t_2) S^\dagger(t_2, 0) \\
&= \mathfrak{h}(t_1) G^>(t_1, t_2) + I_1^>(t_1, t_2).
\end{aligned} \tag{74}$$

where the second equality comes from the Kadanoff-Baym equation for  $G^>$ . This results in

$$i\partial_{t_1} g^>(t_1, t_2) = S^\dagger(t_1, 0) I_1^>(t_1, t_2) S(t_2, 0). \tag{75}$$

Therefore, by integrating from present time  $T_p$  to  $T_p + \Delta$ ,

$$\begin{aligned}
&i [g^>(T_p + \Delta, t_2) - g^>(T_p, t_2)] \\
&= \int_{T_p}^{T_p + \Delta} S^\dagger(\bar{t}, 0) I_1^>(\bar{t}, t_2) S(t_2, 0) d\bar{t} \\
&= S^\dagger(T_p, 0) \int_0^\Delta S^\dagger(\bar{t} + T_p, T_p) I_1^>(\bar{t} + T_p, t_2) S(t_2, 0) d\bar{t}.
\end{aligned} \tag{76}$$

Thus

$$\begin{aligned}
G^>(T_p + \Delta, t_2) &= S(T_p + \Delta, T_p) G^>(T_p, t_2) \\
&- i S(T_p + \Delta, T_p) \int_0^\Delta S^\dagger(\bar{t} + T_p, T_p) I_1^>(\bar{t} + T_p, t_2) d\bar{t}.
\end{aligned} \tag{77}$$

Up to this point we have not made any approximations but merely formal rewritings of the KBE. To calculate the  $S(T_p + \Delta, T_p)$  we divide the interval  $[T_p, T_p + \Delta]$  into  $N$  intervals in which the single-particle Hamiltonian,  $\mathfrak{h}$ , is taken constant and evaluated at the midpoint. For a constant  $\mathfrak{h}$  we obtain

$$\begin{aligned}
S\left(T_p + \frac{(j+1)\Delta}{N}, T_p + \frac{j\Delta}{N}\right) \\
= \exp\left(-i\mathfrak{h}\left(T_p + \frac{(j+1/2)\Delta}{N}\right) \frac{\Delta}{N}\right),
\end{aligned} \tag{78}$$

which is evaluated by diagonalization. The resulting expression becomes

$$S(T_p + \Delta, T_p) = \prod_{j=0}^{N-1} \exp\left(-i\mathfrak{h}\left(T_p + \frac{(j+1/2)\Delta}{N}\right) \frac{\Delta}{N}\right). \tag{79}$$

Given that  $N$  is taken large enough, the only error of the above expression comes from the extrapolation/interpolation of  $\mathfrak{h}$ , which is small as the density (which enters  $\mathfrak{h}$  via the HF term) is a continuous and smooth function of time. To solve Eq. (77) we also need to approximate the integral. This can be done in two different ways depending on which of the two quantities  $I_1^>(\bar{t} + T_p, t_2)$  or  $\tilde{I}_1^>(\bar{t} + T_p, t_2) = S^\dagger(\bar{t} + T_p, T_p) I_1^>(\bar{t} + T_p, t_2)$  is the most slowly varying function. We have tried both and seen that the  $\tilde{I}_1^>(\bar{t} + T_p, t_2)$  is the smoothest. The integral is done numerically, typically with a 2- or 4-point formula. Similar expressions are used for the other KBE. Special attention is needed only for the time diagonal. In this case we combine the two first KBE, Eqs. (54, 55) and using the property in Eq. (64),

$$\begin{aligned}
i[\partial_{t_1} + \partial_{t_2}] G^<(t_1, t_2) &= [\mathfrak{h}, G^<(t_1, t_2)] \\
&+ I_1^<(t_1, t_2) - I_2^<(t_1, t_2),
\end{aligned} \tag{80}$$

we then change to the variables  $t = (t_1 + t_2)/2$  and  $t' = t_1 - t_2$ . This gives

$$\begin{aligned}
i\partial_t G^<(t + t'/2, t - t'/2) &= [\mathfrak{h}, G^<(t + t'/2, t - t'/2)] \\
&+ I_1^<(t + t'/2, t - t'/2) - I_2^<(t + t'/2, t - t'/2)
\end{aligned} \tag{81}$$

By performing the same gauge transformation as above and setting  $t' = t_1 - t_2 = 0$  we obtain<sup>41</sup>

$$i\partial_t g^<(t) = \tilde{I}_1^<(t) - \tilde{I}_2^<(t), \tag{82}$$

where  $\tilde{I}^<(t) = S^\dagger(t, 0) I^<(t, t) S(t, 0)$ . Integrating from time  $T_p$  to  $T_p + \Delta$  we obtain

$$g^<(T_p + \Delta) = g^<(T_p) - i \int_{T_p}^{T_p + \Delta} \left( \tilde{I}_1^<(\bar{t}) - \tilde{I}_2^<(\bar{t}) \right) d\bar{t}, \tag{83}$$

which leads to

$$\begin{aligned}
G^<(T_p + \Delta) &= S(T_p + \Delta, T_p) G^<(T_p) S^\dagger(T_p + \Delta, T_p) \\
&- i S(T_p + \Delta, T_p) \int_0^\Delta \left( \tilde{I}_1^<(\bar{t} + T_p) - \tilde{I}_2^<(\bar{t} + T_p) \right) d\bar{t} \\
&\times S^\dagger(T_p + \Delta, T_p).
\end{aligned} \tag{84}$$

The integral is then evaluated in the same way as discussed above for the case  $t_1 \neq t_2$ .

## VII. TDDFT EXCHANGE-CORRELATION POTENTIAL FROM MBPT

Our time-dependent densities from the different Many-Body Approximations also provide insight for the TDDFT exchange-correlation potentials for strongly correlated systems. Given a specific approximation, from the resulting time-dependent density we obtain the corresponding effective potential  $v_{eff} = \Sigma_H + w + v_{xc}$ , where  $\Sigma_H$  is the Hartree potential and  $v_{xc}$  the exchange correlation potential. In practice, this is done via a numerical reverse engineering procedure.<sup>28</sup> This algorithm imposes that  $|n(R, t) - n^{KS}(R, t)| = 0$  at each time-step, where  $n^{KS}(R, t) = \sum_{\nu}^{occ} |\psi_{\nu}^{KS}(R, t)|^2$  is the Kohn-Sham density and  $\psi_{\nu}^{KS}$  are the Kohn-Sham orbitals. The  $n^{KS}$  is found by solving  $i\hat{\psi}_{\nu}^{KS} = (\hat{t} + v_{eff})\psi_{\nu}^{KS}$  where the kinetic energy is given by  $\hat{t} = -V \sum_{\langle RR' \rangle \sigma} a_{R\sigma}^{\dagger} a_{R'\sigma}$ .

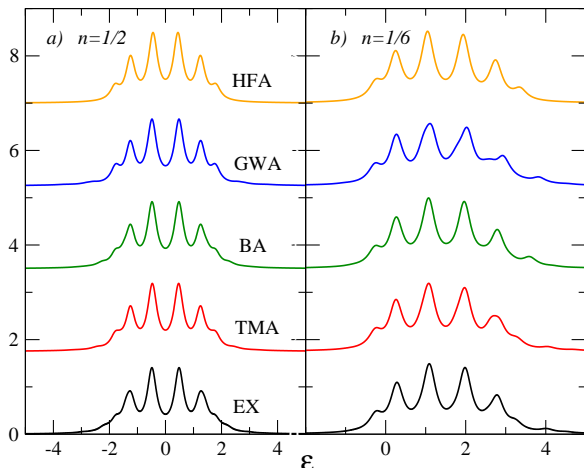


FIG. 4: (Color online) Ground-state spectral functions for  $M=6$  for weak interaction strength,  $U = 1$ , for different fillings. The curves correspond to exact (black), TMA (red), BA (green), GWA (blue) and HFA (orange). The curves are shifted for clearer comparison and we have broadened the discrete spectra with a Lorentzian with a  $FWHM = 0.4$ .

## VIII. RESULTS: GROUND STATE

To start the time propagation of the KBE, one needs the initial, equilibrium, one-particle propagators. These are found by solving the Dyson equation self-consistently. Here, we show only results for isolated clusters, and defer to a future publication the case of clusters contacted to leads. To characterize the ground-state properties, we present in Figs. 4 and 5 the spectral functions at the first,  $R = 1$ , site in the cluster. This is the

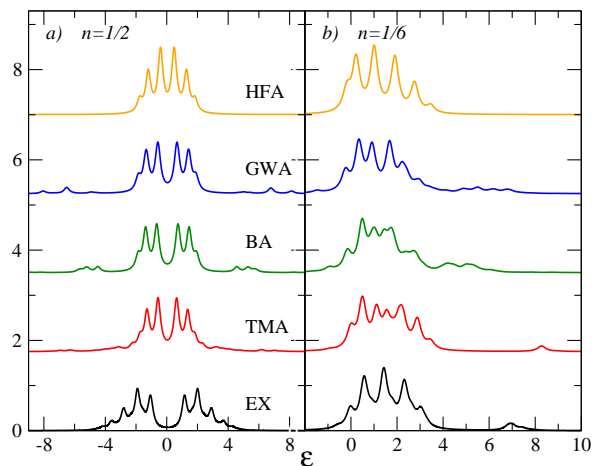


FIG. 5: (Color online) Ground-state spectral functions for  $M=6$  for strong interaction strength,  $U = 4$ , at different fillings. The curves correspond to exact (black), TMA (red), BA (green), GWA (blue) and HFA (orange). The curves are shifted for clearer comparison and we have broadened the discrete spectra with a Lorentzian with a  $FWHM = 0.4$ .

site at which the external perturbation is applied (see section IX). The results are for the different Many-Body Approximations, at two particle concentrations and interaction strengths. A first, general comment is that the performance of MBA:s generally worsens with increasing  $U$ . Some basic, generic features of the different Many-Body Approximations we employ to evolve in time our clusters are already revealed by the ground-state results. Such features, specifically discussed for the cases in Figs. 4 and 5, are common to other clusters with different fillings, sizes and interactions strengths (such additional results are not shown). Fig. 4 refers to the situation of weak interaction, where the performance of the MBA:s is satisfactory (in particular, all the MBA:s reproduce the symmetry breaking at low filling of the exact solution).

At half filling, a correlation gap opens on increasing  $U$ , which becomes clearly visible in the strong correlation regime, Fig. 5. This behavior in clusters is consistent with the exact solution of the 1D Hubbard model in the thermodynamical limit.<sup>42</sup> This feature is reproduced by the different approximate schemes. However, the size of the approximate gap depends on the Many-Body Approximation: the best estimate is given by the BA value; yet, the latter largely underestimates the exact value. Missing the contribution of correlation effects, the non-magnetic HFA solutions reproduce the non-interacting spectral density. As a second general feature, the MBA:s introduce spurious satellites away from the band region. This problem is most pronounced in the BA and GWA curves. In the low density regime, for large  $U$ , a satellite structure appears in the exact solution (about 6.5 in the bottom of panel 4b). In an extended system, this high energy spectral feature represents a two-electron anti-bound state (i.e. outside the band continuum). The

satellite is well reproduced by the TMA (although its distance from the band region is overestimated) while is smeared out in the BA and GWA and obviously absent in the HFA (as it includes no correlation effects). For the strong interaction case, the agreement of the different approximations with the exact curve in the band region is only moderate.

When comparing the SGWA to the GWA we see a slight improvement, which is expected, as the SGWA includes fewer faulty diagrams. This improved version of the GWA is, however, still worse than the BA or the TMA. In this section, we show no results for the SGWA, since it introduces only a marginal improvement in the ground-state spectral density: however, we will present below SGWA time-dependent densities. It is worth noticing that, using a MBA expansion in terms of non-magnetic propagators, the SGWA will have a magnetic instability on increasing  $U$ . This can be seen most easily in a Hubbard dimer with two electrons with opposite spins. In the dimer, where the poles of  $W[G_0]$  are  $\epsilon = \pm\sqrt{4V^2 \pm 2VU}$ , this unphysical symmetry breaking occurs for  $U \geq 2V$ . Conversely, the exact ground state for a dimer is always a spin  $S = 0$  (singlet) state, since, for any positive  $U$ , the dimer ground-state energy  $E_{gs}^{dimer} = E_{dimer}^{S=0} = \frac{U - \sqrt{16V^2 + U^2}}{2} < 0 = E_{dimer}^{S=1}$ .

It is worth noting that all the spectral functions shown in Figs. 4 and 5 are not as good as those obtained without self-consistency, i.e. when stopping after the first iteration of the Dyson equation, see Fig 6. This is an example of the known fact that self-consistent conserving approximations often have worse spectral properties than non self-consistent ones.<sup>43,44</sup> To guarantee the fulfillment of the conservation laws and to get unambiguous total energy results it is capital to achieve self-consistency. If the quantity of interest is the spectral functions one should instead make use of different partial summation criteria,<sup>43</sup> and in some cases include vertex corrections to remove artifacts introduced by self-consistency.<sup>35</sup>

As a final remark to this section we note that all MBA:s based on partial summations involve infinitely many possible excitations. These excitations, represented by diagrams in the self energy, result in infinitely many, but discrete, number of poles in the ground-state spectral functions.<sup>45</sup> The exact solution, in contrast, lives in a finite phase space which implies a finite number of poles.

## IX. RESULTS: TIME DEPENDENCE

In this section we examine the performance of the different MBA:s. To accomplish this, we use as benchmark exact many-body solutions. In general, the latter are available only for finite systems, and numerical in nature. As a consequence, in this section we deal exclusively with isolated clusters, and focus on general aspects of the time-dependent densities and MBA:s. However, we defer to the next section two important outcomes of the KBE time evolution: the correlation-induced damping and the

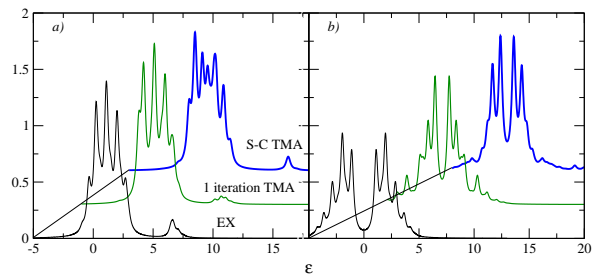


FIG. 6: (Color online) First iteration and self-consistent TMA spectral function versus the exact one.  $M=6$  and in a):  $n = 1/6$  and in b):  $n = 1/2$ . The curves correspond to exact (black), first iteration TMA (green) and self-consistent TMA (thick blue). The curves are shifted for clearer comparison and we have broadened the discrete spectra with a Lorentzian with a  $FWHM = 0.4$ .

existence of multiple steady states in isolated and contacted clusters.

*Isolated clusters: MBA:s vs exact results.* We start the time evolution at  $t = 0$  with the ground-state Green's function. For positive times  $t > 0$  we apply a spin-independent external field to the system. We have studied different types of external fields, but in this paper we present results only for the form  $w_R(t) = w_0 \delta_{R,1} \Theta(t)$ , that is we consider a step perturbation and let it to act only on the leftmost,  $R = 1$ , site. The time is given in units of the inverse hopping parameter ( $1/V$ ) and all curves represent the dynamics on site  $R = 1$ . The cases displayed are the same as those considered for the ground-state results.

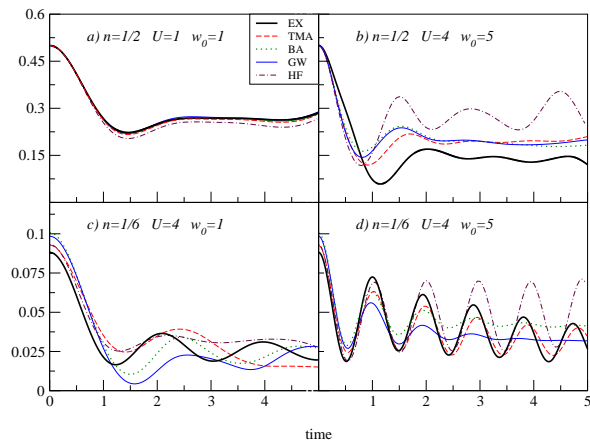


FIG. 7: (Color online) Time-dependent densities on site 1 for  $M = 6$ . The curves correspond to exact (thick solid black), TMA (dashed red), BA (dotted green), GWA (thin solid blue) and HFA (brown dashed dot).

We show the resulting time-dependent densities in Fig. 7. The curves correspond to some initial states shown in Figs. 4 and 5. In the panels a) and b),  $n = 1/2$  while in panels c) and d),  $n = 1/6$ . In the simplest case

( $U = 1, w_0 = 1$ ), presented in panel a), all MBA:s give a good description of the density. On increasing the strength of the interaction and the external field, panel b), we clearly see that the HFA description is rather crude, whilst the curves from the other MBA:s are very similar to each other and closer to the exact density. In the case of strong interaction but weak field, panel c), we see that none of the MBA:s give an adequate description. We interpret these results as a consequence to the fact that the ground-state spectral function is not well described in the band region: the latter is responsible for the response to weak fields. On the contrary, when the field is strong, panel d), the TMA performs much better than the other MBA:s. This is due to the fact that the non-linear response involves states at higher excitation energy and the TMA is the only approximation which, to some extent, reproduces the satellite structure.

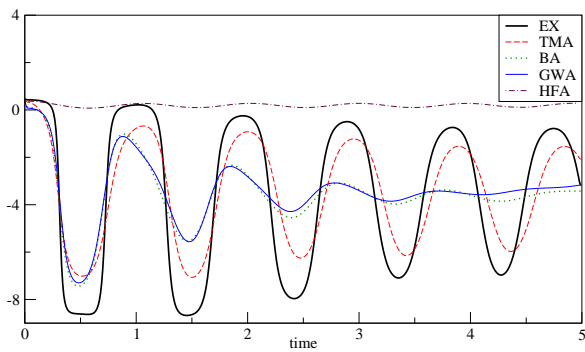


FIG. 8: (Color online) Time-dependent  $v_{eff}$  on site 1 for  $M = 6$ ,  $U = 4$  and  $w_0 = 5$ . The curves correspond to exact (thick solid black), TMA (dashed red), BA (dotted green), GWA (thin solid blue) and HFA (brown dashed dot).

*Isolated clusters: MBA:s, exact results and TDDFT.* It is interesting to examine some of the results just presented from a TDDFT perspective. A clear advantage of TDDFT is that, for the time evolution, it deals with quantities with a single time argument (one is propagating the Kohn-Sham orbitals). Nevertheless, a key requirement in TDDFT is that  $v_{xc}$  (and thus  $v_{eff}$ ) should depend in a non-local (in space and time) fashion on the particle density. In this way, all the complexities of the many-body dynamics are subsumed into a highly non-trivial dependence of  $v_{xc}$  on the density. Not surprisingly, making progress in the construction of improved XC functional is a rather challenging task, especially for strongly correlated systems. It is also true that, in some cases, simple adiabatic local approximations can provide satisfactory results; this is also the case for a TDDFT description of the Hubbard model in non equilibrium.<sup>28,46</sup> However, memory and non-local effects should in general be taken into account. The so-called variational approach to TDDFT,<sup>47,48</sup> has the advantage of a systematic

inclusion of many-body contributions in the XC potential. Also, in this way non-locality in space and memory effects are properly included, once  $v_{xc}$  is retrieved from the many-body self energy via the time-dependent Sham-Schlüter equation.<sup>49</sup> Deferring a "bottom-up" construction of  $v_{xc}$  via MBA:s to future work, we here still wish to explore the connection between TDDFT and MBA:s on the Keldysh contour, looking at exchange-correlation potentials obtained via time-dependent reverse engineering using the time-dependent densities from the KBE. The results of this procedure are presented in in Fig. 8,  $M = 6, N = 2, U = 4, w_0 = 5$ . This corresponds to the time-dependent densities presented in panel d) of Fig. 7. Consistently with the density results, we see the  $v_{eff}$  in the TMA is superior to those from the other MBA:s, and quite close to the exact one. We also note the large discrepancy of the HFA and that, for both the BA and the GWA,  $v_{eff}$  exhibits a damped behavior (the same is observed in the densities in panel d) of Fig. 7, see section X below). In spite of not being perfect, the agreement of  $v_{eff}$  from the TMA with the exact one is quite encouraging, suggesting that there is ample scope for pursuing the construction of improved  $v_{xc}$  from (suitably chosen) MBA:s.

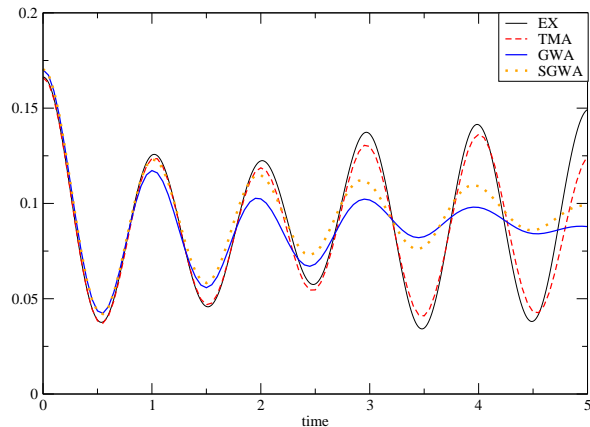


FIG. 9: (Color online) Time-dependent densities for  $M = 4$ ,  $U = 1.5$ ,  $w_0 = 5$  and  $n = 1/4$ . The curves correspond to exact (black), GWA (dotted red), SGWA (thick blue) and TMA (dashed green).

*Spin-dependent GWA.* Before concluding this section, we wish to discuss briefly the effect on making a spin-dependent treatment in the GWA. In Fig. 9, we make a comparison between GWA, SGWA and, for reference, TMA. Due to the symmetry breaking of the SGWA (see section VIII), and that we only consider the spin unpolarized case (otherwise, one should start with polarized propagators) we confine ourselves to the weak interaction regime. As evident from Fig. 9, for the chosen parameters the SGWA is slightly better than its spin-independent counterpart but inferior to the TMA.

As a final remark to this section, we note that in the general case, GWA was designed to give a good screen-

ing of the Coloumb interaction,<sup>20</sup> which in our system has already been taken into account indirectly by the model itself. The TMA, on the other hand, is known to give a good performance if the interaction is short ranged, especially in the low density regime.<sup>21</sup> The general good description of the the TMA (both in and out of equilibrium) for the short-ranged Hubbard Hamiltonian is in accordance to previous studies of ground state properties of clusters.<sup>35,50</sup> One can in other words say that the performance of the different approximations in the ground state has non negligible relevance to the time-dependent behavior of the system, and this is especially the case for two most distinctive spectral features, that is: the band-gap and satellite structure.

## X. RESULTS: DAMPING AND MULTIPLE STEADY STATES

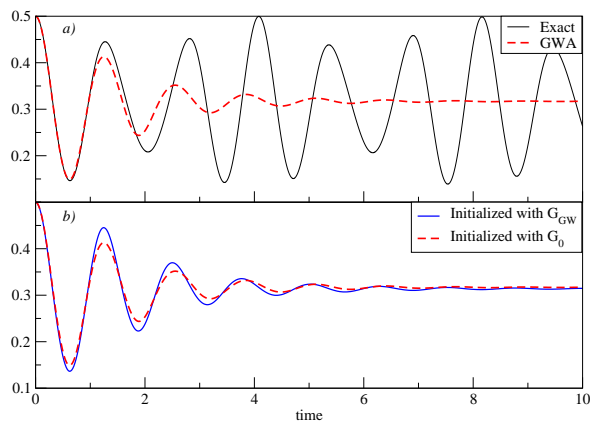


FIG. 10: (Color online) Densities for  $M = 2$ ,  $n = 1/2$ ,  $U = 1$ ,  $w_0 = 5$ , exact (black), GWA (dashed red) and SGWA (blue). In *a*): damping of GWA density versus exact solution. In *b*): time-dependent densities for the GWA, initialized with the self-consistent GWA ground state and the non-interacting  $G_0$ .

In this section we will investigate the correlation-induced damping and the multiple solutions of the stationary KBE. We find that these features are general for all MBA:s which include correlation effects. We exemplify this by presenting results for different MBA:s in the various parts of this section.

When we let our isolated system(s) evolve under the action of a strong external field we reach an artificial steady state,<sup>16,51</sup> see Fig. 10(a). The damping mechanism is not a mere consequence of the infinite number of poles in the initial state but is rather intrinsically linked to the time propagation scheme. To show this fact we present in Fig. 10(b) the time evolved density initiated with the non-interacting propagator  $G_0$ ,<sup>52</sup> which has a finite number of poles. From the curves in Fig. 10(b) it is evident that the non-interacting initial state leads to a

very similar damped density profile. Note that the similarity of the curves in Fig. 10(b), indicate a robustness of the KBE time evolution against the initial conditions.

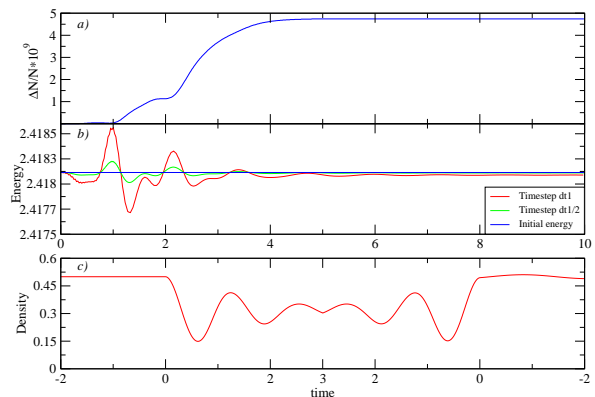


FIG. 11: (Color online) Conservation laws and time reversal in the GWA for  $M = 2$ ,  $n = 1/2$ ,  $U = 1$ ,  $w_0 = 5$ .

The damping is not a numerical artifact: in Fig. 11 we see that particle and energy conservation are strictly obeyed within our numerical accuracy, see top and middle panel. Moreover, the evolution satisfies time-reversal symmetry. That is, when we reverse the direction of time in the propagation, the system goes back to the initial state and remains there, see bottom panel. The damping rate increases with the strength of the external field and is absent in the regime of linear response. The dynamics in this limit is described by the Bethe-Salpeter equation, with a kernel  $\delta\Sigma/\delta G$ . The latter would have a discrete spectrum in our MBA:s, and so would the resulting density response. A discrete response function will in turn lead to a non-damped dynamics. We wish to stress that in a formulation based on conserving Many-Body Approximations, the key quantity is the generating functional; the corresponding  $G$  is then defined via the self-consistent KBE, and not via an underlying wave function scheme. Without the connection to the underlying wave function, there is no guarantee that, for example, systems with a finite phase space will only have a finite number of excited states or that they will not have a damped dynamics.

To study the non-linear response regime, we find convenient to introduce the instantaneous spectral function:

$$A(T_p, \omega) = -\text{Tr} \text{Im} \int_{-2T_p}^{2T_p} e^{i\omega\tau} [G^> - G^<] \left(T_p + \frac{\tau}{2}, T_p - \frac{\tau}{2}\right) d\tau, \quad (85)$$

where  $T_p = (t_1 + t_2)/2$  and  $\tau = (t_1 - t_2)$ , and its counterpart in time space. When reaching the steady state, the spectral function gets broadened in energy space, Fig. 12(a), and damped in time space, Fig. 12(b). Note that, for our dimer, the exact instantaneous spectral function would continue to oscillate in time space. The different MBA:s have different damping rates; among them, the TMA is in general the slowest. The damping acts

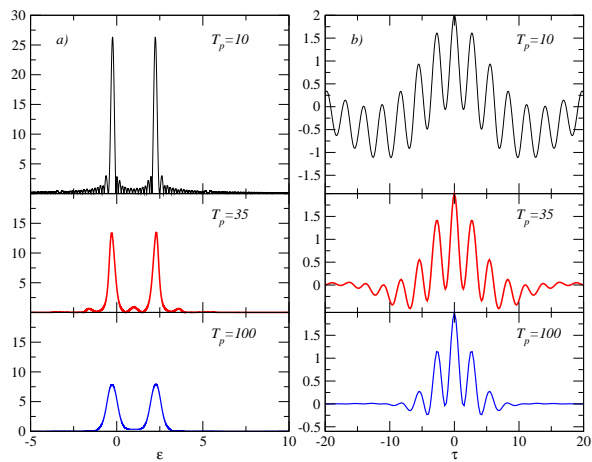


FIG. 12: (Color online) Time-dependent spectral functions in the GWA for  $M = 2$ ,  $n = 1/2$ ,  $U = 1$ ,  $w_0 = 2$ , a): in energy space and b): in time space. The different curves correspond to  $T_p = 10$  (black),  $T_p = 35$  (red) and  $T_p = 100$  (blue).

strongest on the perturbed site, it generally decreases with system size and is most important at half filling. In our study we have not made an exhaustive characterization of how the large-size limit is gradually obtained; this is indeed an issue we plan to address in future work. Still, we wish to present in the rest of this section some general considerations on the effect of system-size on the damping behavior.

*System size and damping.* In an exact treatment, a finite system has a corresponding finite phase space and will thus not be able to fully relax to a stationary steady state. In a large but finite phase space it will, due to decoherence, give rise to a quasi steady state. The larger the system gets, the more and more complete the damping becomes. Thus, after a long time, in an exact time dynamics the system would exhibit noise-like fluctuations which never die but which decrease in amplitude with system size. We have seen that in our approximate KBE evolution the system, while being finite, attains a stationary state. Thus, the artificial damping of the KBE dynamics is expected to increasingly resemble the physical damping as the system grows.

*Self-consistency and damping.* In Many-Body Perturbation Theory, the self energy accounts for possible excitations of the system which involve a certain number of particles/holes. Any MBA based upon partial summations includes diagrams of all orders. These terms act as an effective bath which gives rise to infinitely many discrete poles in the ground state (in isolated systems) and correlation-induced damping in the time dynamics. In a finite system, there will be contributions to the self energy which annihilate more holes/particles than those which can be accommodated in the system. In an exact theory, these unphysical terms would be exactly canceled, order by order, by other unphysical pieces. In approximations such as the GWA or the TMA, there is in general no

such perfect compensation. The infinite number of poles of the ground state and the correlation-induced damping will thus be artificial for a finite system.

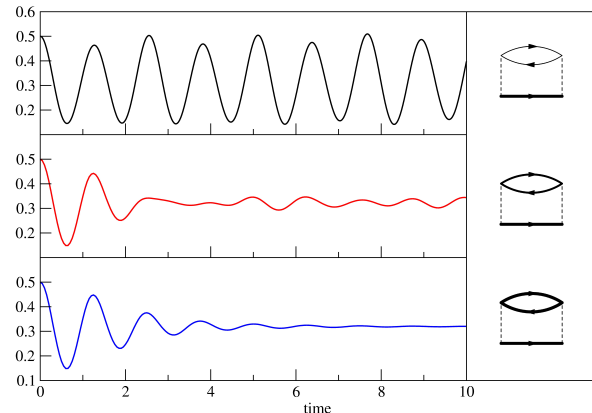


FIG. 13: (Color online) Time-dependent densities for Born approximations with different levels of self-consistency for  $M = 2$ ,  $n = 1/2$ ,  $U = 1$ ,  $w_0 = 5$ ;  $BA_0$  (black),  $BA_{HFA}$  (red) and  $BA$  (blue).

In Fig. 13, we present results from three versions of the BA to illustrate the effect of an increasing level of self-consistency. These approximations, which are all particle-conserving,<sup>53</sup> involve different polarization propagators. In the first case we evaluate the polarization propagator with ground-state propagators ( $BA_0$ ) (top panel). In this case the density does not damp. In the second case we evaluate the polarization with propagators in the time-dependent HFA approximation ( $BA_{HFA}$ ) (middle panel). In this case we observe partial damping. If we finally use the self-consistent  $G$  ( $BA$ ) (bottom panel), we get complete damping. We see in other words that if all  $G$ :s that build up the self energy are the self-consistent ones we reach a steady state.<sup>54</sup>

*Multiple steady states.* Another striking feature related to the correlation-induced damping is that the steady state is not unique for a given final external field: it depends on how the perturbation is switched on. In our simulations, in the case of adiabatic turn-on, we reach the ground state of a system with an on-site energy corresponding to the final external perturbation. This is consistent with the adiabatic theorem. If, however, the perturbation is switched on suddenly, we reach a non-physical steady state with the same energy as at  $t = 0^+$ . This non uniqueness is indicative of an important aspect: given a final external potential, there are multiple, in principle infinitely many, solutions of the stationary KBE in finite clusters. Furthermore, as we show next, this general statement, in some cases, remains valid in presence of macroscopic leads, where we have both a self energy  $\Sigma_{emb}$  from the leads and a self energy  $\Sigma_{MBA}$  from the interactions. Both contributions are non-local in time and may lead to damping. Thus, in general we have two damping mechanisms: One due to the coupling to the

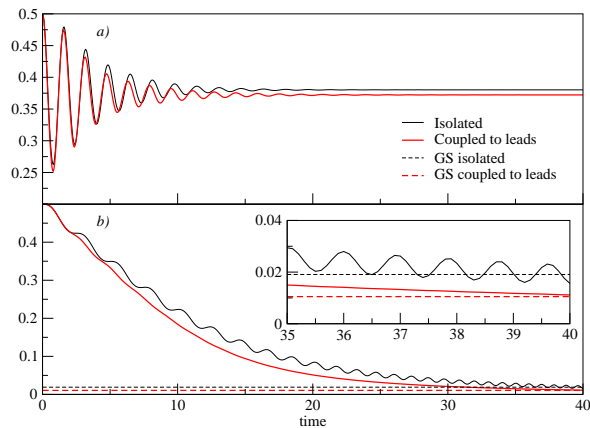


FIG. 14: (Color online) Time-dependent densities for a cluster isolated and coupled to leads in the TMA with sudden and slow switch-on.  $M = 2$ ,  $U = 1$ ,  $w_0 = 8$ . Lead parameters:  $V_L = 1$ ,  $V_{LC} = 0.5$ , filling = 0.5 and bias = 0. *a)* Sudden switch-on: isolated cluster (thin black), coupled to leads (thick red). *b)* Slow switch-on: isolated cluster (thin black), coupled to leads (thick red); ground-state densities of final Hamiltonian: isolated cluster (dashed black), coupled to leads (dashed thick red). *Inset:* expanded view of the long time limit behavior.

continuous lead band and one induced by correlations.

In Fig. 14 we present the time-dependent densities within the TMA for a dimer, both isolated and coupled to unbiased leads,<sup>55,56</sup> subject to an external field with sudden and slow ( $w(t) = w_0 t/t_{max}$ ) switch-on, (panel *a*) and panel *b*) respectively).

The strength of the perturbation is such that the ground state corresponding to the final external potential contains states outside the band continuum (bound states); in this case we find that the KBE admit multiple steady-state solutions.<sup>57</sup> These steady states vary continuously with the way the final potential is reached. In other words we have infinitely many steady states where similar switch-ons give similar steady states. In the case of the HFA we see that the density continues to oscillate if we have more than one pole in the ground state of the final Hamiltonian. This results is consistent with recent work on the role of bound states in quantum transport.<sup>58-61</sup> However, we wish to remark that, in the HFA, the frequency, amplitude and average value of the oscillating density will, however, depend on the way the external field is switched on.<sup>62</sup>

Similarly to the isolated case, we find that for a slow switch-on we tend to reach the ground state corresponding to the final Hamiltonian (given by the dashed curves), while for the sudden switch-on we reach another steady state. If the external field is such that the corresponding ground state of the final Hamiltonian includes only excitations within the band then the steady state reached is the final ground state, independently on how the perturbation is switched on.

The damping induced by correlations and the one due

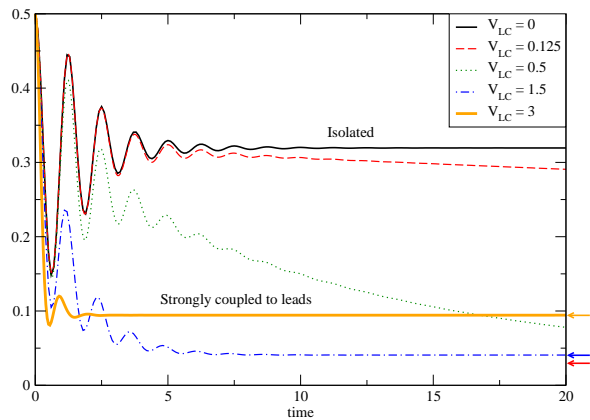


FIG. 15: (Color online) Time-dependent densities for a cluster with different couplings to unbiased leads in the BA.  $M = 2$ ,  $U = 1$ ,  $w_0 = 5$ ,  $V_L = 5$ .

to the coupling to the macroscopic contacts have in general different characteristic time scales. This is clearly seen in Fig. 15 where we have gradually increased the coupling to the leads: here, the external field and the lead band width are such that the corresponding ground state of the final Hamiltonian contains no poles. In the case of an isolated cluster ( $V_{LC} = 0$ ), the damping is only due to correlations. Once the coupling to the leads is non-zero, there will be, in addition to the correlation-induced one, a damping due to the contacts; the latter will eventually bring the system to the corresponding ground state. In Fig. 15, the ground-state values of the densities are represented by arrows (on the scale of the figure, the red and green arrows are not distinguishable). Note that each curve in Fig. 15 corresponds to a different system, i.e. with a different device-lead coupling strength. Each of these systems has a different final Hamiltonian, i.e. a different corresponding ground state. When the coupling strength is weak ( $V_{LC} = 0.125, 0.5$ ), the time scale of the damping due to the leads is much longer than correlation-induced one. For intermediate coupling strengths ( $V_{LC} = 1.5$ ), the characteristic times will be of the same order of magnitude and the interplay of the two mechanisms becomes intrinsically difficult to discern. When the coupling strength is strong ( $V_{LC} = 3$ ), the damping is completely dominated by the leads.

As a final remark, we know that the correlation-induced damping is artificial in isolated clusters, and we saw in Fig. 15 that when the coupling to the leads is weak, the initial damping is also dominated by correlations. These two facts together seem to cast some doubt on the capability of the KBE+MBA:s scheme to describe (within the simple MBA:s discussed here) transients in the weak coupling case (a regime which is of high experimental interest, and in fact among the most investigated in the literature).

To summarize this section, we see that correlation-induced damping and multiple steady states are present

both in isolated and contacted clusters. In the case of isolated clusters, this damping is artificial as the exact solution does not reach a steady state. The question whether or not the correlation-induced damping and the existence of multiple steady states in a cluster coupled to leads is an artifact of Many-Body Perturbation Theory is beyond the scope of this paper and is left to future work.

## XI. CONCLUSIONS AND OUTLOOK

A main objective of this paper has been to describe in detail a method, within the framework of the time-dependent Kadanoff-Baym equations (KBE), to study finite systems in equilibrium as well as out of equilibrium. The main emphasis of the paper has been on finite clusters, for which a meromorphic representation of the equilibrium many-body quantities is possible, but, in few instances, we have also considered some results for contacted clusters.

As a concrete application, we examined the time evolution of clusters with strong, short ranged electron interactions within several Many-Body Approximations, and compared the results to exact ones. A first main outcome of this comparisons is that, for short ranged, Hubbard-type interactions, the T-matrix approximation performs very well at low densities, and is in general superior to the GW and second Born approximations, both in describing the time-dependent density and the corresponding exchange-correlation potential.

A second important outcome of our work is the existence of two remarkable features of the time-dependent KBE. The first is that the KBE present a correlation-induced damping in the non-linear regime. The second is that the steady state reached is in general not unique, i.e. the stationary KBE support multiple stationary states. Since a finite cluster subject to a non-adiabatic perturbation will oscillate indefinitely, it is clear that, for finite systems, such damping and multiple steady-state behavior are artificial. We argue that this shortcomings will always be present when applying infinite order perturbation theory based on partial summations to finite systems. In this paper, we were not able to provide a conclusive answer to whether such two aspects of the KBE bear any physical meaning or if they are a spurious effect of MBPT. As we discuss next, this is part of our plans for follow-up work.

Future research activity may be envisaged in various directions. On the methodological side, it would be of interest to further investigate, for contacted systems, how sound the correlation-induced damping and the multiple steady states are.<sup>64</sup>

A second methodological issue we are currently addressing is performance of the different MBA:s in quantum transport geometries. We will do by comparing the approximate results with those of time-dependent density-matrix renormalization group calculations.<sup>65</sup>

Another possible line of study would be searching for

algorithms to reduce/optimize the computational costs of time-dependent KBE numerical calculations. This is necessary to deal with more realistic systems.

As a fourth direction, it would be of great interest to study the effect of including bosonic degrees of freedom as vibration phenomena often play an crucial role in quantum transport.

Finally, we also intend to use our KBE-based computational treatments in some specific applications: Possible examples are real-time qubit manipulation, bistability induced by electron-phonon interaction, cold-atom dynamics. More specific details are deferred to future publications.

## Acknowledgments

Fruitful discussions with Ulf von Barth, Gianluca Stefanucci and Robert van Leeuwen are gratefully acknowledged. This work was supported by the EU 6th framework Network of Excellence NANOQUANTA (NMP4-CT-2004-500198) and the European Theoretical Spectroscopy Facility (INFRA-2007-211956).

## APPENDIX A: Energy functionals

The energy functionals considered here are the Galitskii-Migdal (GM) and the Luttinger-Ward (LW). An important difference between them is that the GM needs only the knowledge of the single-particle Hamiltonian and of the spectral function of  $G$ , while the LW incorporates the  $\Phi$  functional as well as  $\Sigma[G]$ , which depends on which approximation one is using. Here we give the expression for the LW functional for the GW-approximation. In practice, we evaluated the LW only in the ground state, i.e. in frequency space, while the GM was also used during time evolution.

### a. Galitskii-Migdal

In frequency space, the GM functional reads<sup>66</sup>

$$E = -\frac{i}{2} \text{Tr} \{(\epsilon + h) G\}, \quad (\text{A-1})$$

where  $\text{Tr}$  stands for trace<sup>67</sup> and  $h$  is the single-particle Hamiltonian *not* including  $\Sigma_{HF}$ . Thus

$$E = \sum_R \sum_{i=1}^{n_F} a_i A_{RR}^i - \sum_{RR'} \sum_{i=1}^{n_F} A_{RR'}^i h_{RR'}, \quad (\text{A-2})$$

where  $n_F$  is the number of poles below the Fermi energy, and after having made use of the meromorphic representation of  $G^<$ . In time space, the form of E becomes

$$E = -\frac{i}{2} \text{Tr} [(i\partial_t + h) G^<(t, t^+)]. \quad (\text{A-3})$$

Making use of the the equation of for  $G$ , we obtain

$$E = -\frac{i}{2}\text{Tr} [hG^<(t, t^+)] - \frac{i}{2}\text{Tr} [(h + \Sigma_{HF})G^<(t, t^+) + I_1^<(t, t^+)]. \quad (\text{A-4})$$

*b. Luttinger-Ward*

The LW energy functional is<sup>68</sup>

$$iE = \Phi - \text{Tr} \{ \Sigma G + \ln(\Sigma - G_0^{-1}) \}, \quad (\text{A-5})$$

where the self energy depends functionally on the input  $G$  i.e.  $\Sigma = \Sigma[G]$  and  $\Phi$  is the generating (of the MBA:s) functional. Specializing to the case of the GW approximation, the  $\Phi$  functional becomes

$$\Phi_{GW} = \Phi_{HF} + \frac{1}{4}\text{Tr} \{ \ln[1 - UP] + UP \}, \quad (\text{A-6})$$

where  $\Phi_{HF} = (i/2)\text{Tr} \{ \Sigma_{HF}[G]G \}$ . When computing the logarithmic term  $\ln(\Sigma - G_0^{-1})$  in Eq. (A-5), it is useful to make the following separation

$$\ln[\Sigma - G_0^{-1}] = \ln[-G_{HF}^{-1}] + \ln[1 - G_{HF}\Sigma_c], \quad (\text{A-7})$$

where  $G_{HF}^{-1} = \epsilon - \mathfrak{h}$  and  $\mathfrak{h}$  incorporates the the Hartree and Fock terms and where  $\Sigma_c$  is the correlation part of the GW self energy. The first term in Eq. (A-7) is the sum of the eigenvalues of the occupied Hartree-Fock single-particle states (calculated from the correlated Green's function) which obviously does not correspond to the Hartree-Fock energy. The second contribution in Eq. (A-7) can be evaluated with a well known identity<sup>69</sup>:

$$\begin{aligned} \ln[1 - G_{HF}\Sigma_c] &= -\int_0^1 \frac{G_{HF}\Sigma_c}{1 - \lambda G_{HF}\Sigma_c} d\lambda \\ &= -\int_0^1 \tilde{G}\Sigma_c d\lambda. \end{aligned} \quad (\text{A-8})$$

In Eq. (A-8),  $\tilde{G}$  satisfies the Dyson equation

$$\tilde{G} = G_{HF} + \lambda G_{HF}\Sigma_c\tilde{G}. \quad (\text{A-9})$$

The other logarithmic term in  $\Phi_{GW}$ , i. e.  $\ln[1 - UP]$ , is treated in a similar way. In the actual calculation, expressions of the form  $\text{Tr}[AB]$  are evaluated analytically, whilst integrals of the kind  $\int_0^1 ABd\lambda$  are performed numerically.

- 
- <sup>1</sup> L. P. Kadanoff and G. Baym, *Quantum Statistical Mechanics* (Benjamin, New York, 1962).  
<sup>2</sup> L. V. Keldysh, Zh. Eksp. Teor. Fiz. **47**, 1515, 1964 [Sov. Phys. JETP **20**, 1018 (1965)].  
<sup>3</sup> P. Danielewicz, Ann, Physics **152**, 239 (1984).  
<sup>4</sup> See, for example, *Progress in Nonequilibrium Green's Functions III*, J. Phys. Conf. Ser. **35**, edited by M. Bonitz and A. Filinov (2006).  
<sup>5</sup> N.-H. Kwong and M. Bonitz, Phys. Rev. Lett. **84**, 1768 (2000).  
<sup>6</sup> A.P. Jauho, in Reference<sup>4</sup>, p. 313.  
<sup>7</sup> G. Stefanucci, C.-O. Almbladh, Phys. Rev. B **69**, 195318 (2004).  
<sup>8</sup> N. E. Dahlen, R. van Leeuwen, and A. Stan in Reference<sup>4</sup>, p. 340.  
<sup>9</sup> K. Balzer, M. Bonitz, R. van Leeuwen, A. Stan, N. E. Dahlen, Phys. Rev. B **79**, 245306 (2009).  
<sup>10</sup> M. Galperin, A. Nitzan, M.A. Ratner, Phys. Rev. B **76**, 035301 (2007).  
<sup>11</sup> K. S. Thygesen and A. Rubio, Phys. Rev. B **77**, 115333 (2008).  
<sup>12</sup> P. Darancet, A. Ferretti, D. Mayou, V. Olevano Phys. Rev. B **75**, 075102 (2007).  
<sup>13</sup> P. Myöhänen, A. Stan, G. Stefanucci and R. van Leeuwen, Eur. Phys. Lett. **84**, 67001 (2008).  
<sup>14</sup> P. Myöhänen, A. Stan, G. Stefanucci and R. van Leeuwen, Phys. Rev. B **80**, 115107 (2009).  
<sup>15</sup> J.K. Freericks, Phys. Rev. B **77**, 075109 (2008).  
<sup>16</sup> M. Puig von Friesen, C. Verdozzi and C.-O. Almbladh, Phys. Rev. Lett. **103**, 176404 (2009).  
<sup>17</sup> See, for example, T. H. Oosterkamp, T. Fujisawa, W. G. van der Wiel, K. Ishibashi, R. V. Hijman, S. Tarucha and L. P. Kouwenhoven, Nature **395**, 873 (1998).  
<sup>18</sup> B.T. Seaman, M. Kramer, D.Z. Anderson, and M.J. Holland, Phys. Rev. A **75**, 023615 (2007).  
<sup>19</sup> A short account of this work was reported previously.<sup>16</sup>  
<sup>20</sup> L. Hedin, Phys. Rev. **139**, A796 (1965).  
<sup>21</sup> V. Galitskii, Soviet Phys. JETP **7**, 104 (1958).  
<sup>22</sup> D. Semkat, D. Kremp, M. Bonitz, Contributions to Plasma Physics, **42**, 31 (2002).  
<sup>23</sup> K. S. Thygesen, Phys. Rev. Lett. **100**, 166804 (2008).  
<sup>24</sup> P. Romaniello, D. Sangalli, J. A. Berger, F. Sottile, L. G. Molinari, L. Reining and G. Onida, J. Chem. Phys. **130**, 044108, (2009).  
<sup>25</sup> W. Nelson, P. Bokes, Patrick Rinke and R.W. Godby, Phys. Rev. A **75**, 032505 (2007).  
<sup>26</sup> E. Runge and E. K. U. Gross, Phys. Rev. Lett. **52**, 997 (1984).  
<sup>27</sup> R. van Leeuwen, N. E. Dahlen, G. Stefanucci, C. O. Almbladh, and U. von Barth, *Time-Dependent Density Functional Theory* (Springer, New York, 2006) and references therein.  
<sup>28</sup> C. Verdozzi, Phys. Rev. Lett. **101**, 166401 (2008).  
<sup>29</sup> This condition also applies to the first argument.  
<sup>30</sup> In extended Coulomb systems,  $w$  and the Hartree potential  $\Sigma_H$  are infinite but with a finite sum and must be treated together. In this work we consider model systems with short-range interactions and such a procedure is not mandatory.  
<sup>31</sup> In the spin-independent treatment  $P = \sum_{\sigma} P_{\sigma}$ .  
<sup>32</sup> There exist also contributions coming from ladder diagrams with interactions only/also in the electron-hole

- channel, usually of principal relevance in exciton-type problems; however, such contributions are not the dominant ones in the low-density limit for our Hubbard clusters with one orbital/site; and in the rest of the paper, we do not consider them altogether, limiting ourselves to particle-particle or hole-hole ladder contributions.
- <sup>33</sup> S. Datta, *Electronic Transport in Mesoscopic Systems* (Cambridge UP, Cambridge, 1995).
- <sup>34</sup> H. Haug and A.-P. Jauho, *Quantum Kinetics in Transport and Optics of Semiconductors*, (Springer, Berlin, 1996).
- <sup>35</sup> M. Cini and C. Verdozzi, *Nuovo Cimento D* **9**, 1 (1987).
- <sup>36</sup> The Dyson equations for  $T$  or  $W$  are solved in a similar way.
- <sup>37</sup> In the case of complex time arguments we would have  $G(12) = -G(2^*1^*)^\dagger$ . This will henceforth be implicit in all similar symmetry relations.
- <sup>38</sup> The  $T^>(t, t)$  is also needed as there is no closed relation to  $T^<(t, t)$ .
- <sup>39</sup> H. S. Köhler, N. H. Kwong, and H. A. Yousif *Comp. Phys. Comm.* **123**, 123 (1999).
- <sup>40</sup> In general it would correspond to the occupation numbers of the single-particle basis.
- <sup>41</sup> Explicit reference to the two-time dependencies is omitted as  $t_1 = t_2$ .
- <sup>42</sup> E.H. Lieb and F.Y. Wu, *Phys. Rev. Lett.* **20**, 1445 (1968).
- <sup>43</sup> C.-O Almladh, in Reference<sup>4</sup>, p. 127.
- <sup>44</sup> B. Holm, U. von Barth, *Phys. Rev. B* **57**, 2108 (1998).
- <sup>45</sup> Continuous broadened ground-state spectral functions have been found for few electron quantum dots<sup>9</sup>, in contrast, for the systems considered here our results show only discrete spectral features.
- <sup>46</sup> W. Li, G. Xianlong, C. Kollath and M. Polini, *Phys. Rev. B* **78**, 195109 (2008).
- <sup>47</sup> C.-O. Almladh, U. von Barth and R. van Leeuwen, *Int. J. Mod. Phys. B* **13**, 535 (1999).
- <sup>48</sup> U. von Barth, N. E. Dahlen, R. van Leeuwen, and G. Stefanucci, *Phys. Rev. B* **72**, 235109 (2005).
- <sup>49</sup> R. van Leeuwen, *Phys. Rev. Lett.* **76**, 3610 (1996).
- <sup>50</sup> C. Verdozzi, R. W. Godby, S. Holloway, *Phys. Rev. Lett.* **74**, 2327 (1995).
- <sup>51</sup> In a steady state all the single-particle properties are independent of time and the one-particle Green's function depends only on the time difference, i.e.  $G(t, t') \rightarrow G(t - t')$ .
- <sup>52</sup> Initializing with  $G_0$  corresponds to a sudden switch-on of the interaction as well as of the external field.
- <sup>53</sup> U. von Barth, unpublished.
- <sup>54</sup> This conclusion applies to all MBA:s here, although partially self-consistent, but particle-conserving schemes can be easily devised for GWA but not for TMA.
- <sup>55</sup> The theoretical formulation to treat macroscopic leads within the Keldysh formalism will be presented in detail in a future paper.
- <sup>56</sup> The hopping parameter in the central region is, similarly to the isolated case, set to unity throughout the paper.
- <sup>57</sup> The existence of multiple steady states remains valid in the case that we apply a bias to the leads.
- <sup>58</sup> A. Dhar, D. Sen, *Phys. Rev. B* **73**, 085119 (2006).
- <sup>59</sup> G. Stefanucci, *Phys. Rev. B* **75**, 195115 (2007).
- <sup>60</sup> For a review, see E. Khosravi, S. Kurth, G. Stefanucci, E.K.U. Gross, *Appl.Phys. A* **93**, 355 (2008).
- <sup>61</sup> C. Verdozzi, G. Stefanucci, C.-O. Almladh, *Phys. Rev. Lett.* **97**, 046603 (2006). In this paper, of a self-consistent oscillatory solution was observed in a short wire with Holstein-type phonons, and connected to 1D noninteracting leads.
- <sup>62</sup> In the case of  $U = 0$  the frequency is independent of the switch-on.<sup>59</sup>
- <sup>63</sup> U. von Barth, N. E. Dahlen, R. van Leeuwen, and G. Stefanucci, *Phys. Rev. B* **72**, 235109 (2005).
- <sup>64</sup> Should these features of the KBE turn out to be artificial, one could try to find ways to suppress the non-physical behavior while keeping the connection to MBPT. One possibility could be to use the variational properties of the underlying  $\Phi$  functional and use the Sham-Schlüter equation to determine on the fly the corresponding TDDFT potentials. At full self-consistency, the TDDFT dynamics would just reproduce the damped KBE dynamics. If one instead use optimized one-particle  $G$  when constructing the exchange correlation potential,  $v_{xc}$ .<sup>47,63</sup>, we expect that the non-physical damping will be reduced or removed without seriously deteriorating the short-time dynamics. In the BA, this approach consists in using a (time-) optimized independent-particle  $G$  when constructing the self energy and  $v_{xc}$  and in section X we saw that the damping is indeed reduced. The use of MBPT based TDDFT potentials could be of great importance of its own due to the possibility of treating larger and more complex systems.
- <sup>65</sup> See, for example, P. Schmitteckert *Phys. Rev. B* **70**, 121302(R) (2004).
- <sup>66</sup> V. M. Galitskii and A.B. Migdal, *Zh. Eksp. Teor. Fiz.* **34**, 139 (1958) [*Sov. Phys. JETP* **139**, 96 (1958)].
- <sup>67</sup> In frequency space  $\text{Tr} \equiv 2 \lim_{\eta \rightarrow 0^+} \sum_{RR'} \delta_{RR'} \int \frac{d\epsilon}{2\pi} e^{i\epsilon\eta}$  and in time space  $\text{Tr} \equiv 2 \sum_{RR'} \delta_{RR'}$ . The space in which the expressions are represented are given by the context.
- <sup>68</sup> J.M. Luttinger and J.C. Ward, *Phys. Rev.* **118**, 1417 (1960).
- <sup>69</sup> P. Güttinger, *Z. Phys.* **73**, 169 (1932).